Toxicology 501 (2024) 153686

Contents lists available at ScienceDirect

Toxicology

journal homepage: www.elsevier.com/locate/toxicol

A mechanistic toxicology study to grasp the mechanics of zearalenone estrogenicity: Spotlighting aromatase and the effects of its genetic variability

Florinda Perugino [a,b,1], Lorenzo Pedroni [a,1], Gianni Galaverna [a], Chiara Dall'Asta [a], Luca Dellafiora [a,*]

[a] Department of Food and Drug, University of Parma, Parma, Italy
[b] Department of Biology, University of Naples Federico II, Naples, Italy

ARTICLE INFO

Handling Editor: Mathieu Vinken

Keywords:
Zearalenone
α-zearalenol
Aromatase
CYP19A1
Xenoestrogen
Mycotoxin
Toxicity
Molecular modelling

ABSTRACT

Zearalenone (ZEN) is a mycoestrogen produced by *Fusarium* fungi contaminating cereals and in grain-based products threatening human and animal health due to its endocrine disrupting effects. Germane to the mechanisms of action, ZEN may activate the estrogen receptors and inhibit the estrogens-producing enzyme aromatase (CYP19A1). Both show single nucleotide variants (SNVs) among humans associated with a diverse susceptibility of being activated or inhibited. These variations might modify the endocrine disrupting action of ZEN, requiring dedicated studies to improve its toxicological understanding. This work focused on human aromatase investigating via 3D molecular modelling whether some of the SNVs reported so far (n = 434) may affect the inhibitory potential of ZEN. It has been also calculated the inhibition capability of α-zearalenol, the most prominent and estrogenically potent phase I metabolite of ZEN, toward those aromatase variants with an expected diverse sensitivity of being inhibited by ZEN. The study: i) described SNVs likely associated with a different susceptibility to ZEN and α-zearalenol inhibition - like T310S that is likely more susceptible to inhibition, or D309G and S478F that are possibly inactive variants; ii) proofed the possible existence of inter-individual susceptibility to ZEN; iii) prioritized aromatase variants for future investigations toward a better comprehension of ZEN xenoestrogenicity at an individual level.

1. Introduction

Zearalenone (ZEN; Fig. 1) is a mycotoxin produced by fungi belonging to the *Fusarium* genus (mainly *F. culmorum* and *F. graminearum*) (EFSA, 2011; Malir et al. 2023) and it is among those most relevant to food safety due to its toxicity and high incidence in food and feed commodities (Catteuw et al. 2019; Silva et al. 2019). Indeed, ZEN is often present in various food and feed ingredients such as corn and wheat, and some food pose a higher risk to unintended ZEN consumption, including whole meal cereals and certain gluten-free products (Jing et al. 2022; Pfleger and Schwake-Anduschus, 2023).

ZEN has shown an endocrine disrupting activity *in vivo* as animal studies reported its capability to impair hormonal balance (Kowalska et al. 2016). In humans, evidence have pointed to a series of disorders associated with the dietary exposure to ZEN, including effects on girls' growth, precocious puberty and thelarche/mastopathy development (Massart et al. 2008; Massart and Saggese, 2010; Rai et al. 2020; Rivera-Nunez et al. 2019). It was also hypothesized that ZEN can be associated with cancer development/progression (Claeys et al. 2020; Ekwomadu et al. 2022; Lo et al. 2023; Rong et al. 2022), though it has been defined as not classifiable as carcinogenic to humans due to the limited evidence in experimental animals (Claeys et al. 2020; IARC, 1993). Germane to the mechanisms of toxicity, ZEN estrogenicity may rely on its concerted capability to activate estrogen receptors (ERs) and inhibit aromatase (CYP19A1) (EFSA, 2011; Wang et al. 2014). From a structural standpoint, ZEN is a resorcylic acid lactone (molecular

Abbreviations: αZAL, α-zearalanol; αZEL, α-zearalenol; ERs, estrogen receptors; ZEN, zearalenone; TES, testosterone; NAR, naringenin; SNVs, single nucleotide variants; WT, wild-type; MD, molecular dynamics.

* Correspondence to: Department of Food and Drug, University of Parma, Parco Area delle Scienze 27/A, 43124 Parma, Italy.
E-mail address: luca.dellafiora@unipr.it (L. Dellafiora).

[1] These authors contributed equally to this work

https://doi.org/10.1016/j.tox.2023.153686
Received 13 October 2023; Received in revised form 23 November 2023; Accepted 25 November 2023
Available online 28 November 2023

formula C18H22O5) whose structure resembles that of the endogenous estrogen 17β-estradiol (E2). This similarity allows for a (partial) agonistic behaviour of ZEN versus ERs, which can be bound and activated eventually eliciting an estrogenic response (EFSA, 2011). Similarly, the structural analogies to steroids make ZEN suitable to compete also with aromatase substrates/products resulting in its inhibition (Wang et al. 2014). This event may lead to a ZEN-dependent reduction of E2 production being aromatase responsible for the conversion of androgens to estrogens (Rizner and Romano, 2023). The final balance of these two apparently contradictory effects concurs in the determination of the final estrogenic potency of ZEN. Moreover, it has been proved that the sensitivity to ZEN-dependent estrogenic insult may depend on the phase I metabolism of ZEN and specifically on the production of α-zearalenol (αZEL). αZEL is part of the chemical complex found in contaminated foodstuff (De Boevre et al. 2013), but it is also the predominant ZEN phase I metabolite in humans, and it has shown a xenoestrogenic activity way more potent than ZEN (Gupta et al. 2022). With this respect, animal species able to predominantly produce αZEL over the other ZEN phase I metabolites are typically associated with strong sensitivity to ZEN exposure (Knutsen et al. 2017). Moreover, a close structural analogue of αZEL, i.e. the α-zearalanol (αZAL), has also been proved to inhibit aromatase although with a lower efficiency compared to ZEN (Wang et al. 2014), suggesting that αZEL might have a certain degree of aromatase inhibitory potential as well.

ERs and aromatase show single nucleotide variants (SNVs) among individuals which may impact their inherent activity and functions (Katzenellenbogen et al. 2018; Simpson, 2000). In this respect, the present work investigated SNVs of aromatase being the ZEN-dependent inhibition of aromatase still largely overlooked though crucial to better characterize the toxicodynamic of ZEN. Specifically, it has been proved that SNVs of aromatase may have a diverse activity and susceptibility of being inhibited compared to the wild-type (WT) enzyme (Kao et al. 1998; Russell et al. 2014). This background information suggests that the inhibitory effects of ZEN might change depending on the aromatase variant, which in turn might impact the disrupting activity of ZEN in individuals depending on the aromatase variant they express. These aspects, the analysis of which targets the toxicodynamic of ZEN from a "personalised" standpoint, are still largely overlooked though they might enforce the background information of ZEN toxicology. The clarification of these aspects is desirable either to boost the understanding of ZEN action among the human population or to improve the assessment of ZEN-associated risk at an individual level.

Specifically, the study targeted the whole set of human aromatase SNVs available in UniProt (www.uniprot.org) (Bateman et al. 2023) at the time of analysis (i.e. 434 variants; last database access 25th September 2023), focusing on those surrounding the ligand binding pocket (15 SNVs) being most likely to affect the interaction of ZEN and αZEL. From a methodological standpoint, computational approaches already proved to be successful, and their application is getting broader and able to cope with several aspects of the food science field (Ji et al. 2020; Wang et al. 2022; Zhao et al. 2021). Specifically, this study relied on a well-established *in silico* workflow integrating docking studies and molecular dynamics to simulate the binding event and the stability of ligand-aromatase complex over the time as a mean to study the effects of SNVs on aromatase inhibition by ZEN. In this respect, evidence previously collected have proven that this analytical approach succeeded to

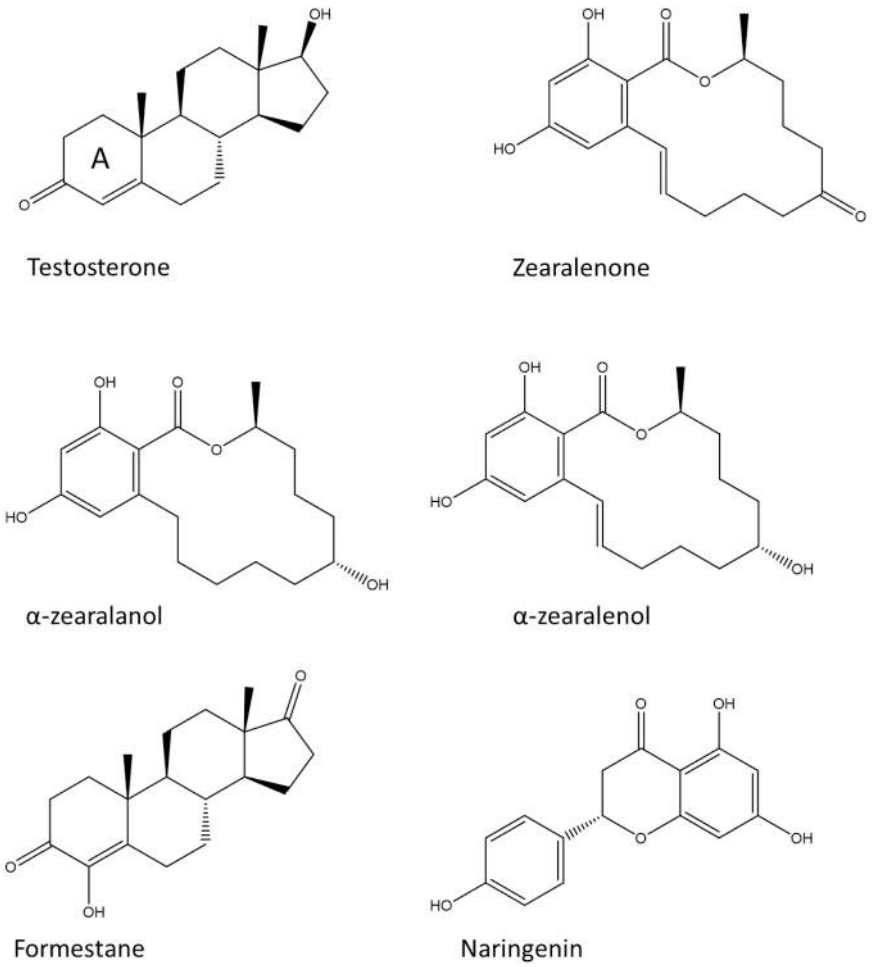

Fig. 1. Chemical structure of molecules under analysis.

estimate effectively whether mutations affect the protein-ligand complex formations (Dorne et al. 2022; Louisse et al. 2022), turning out to be particularly suitable for this case study.

Overall, the study described aromatase SNVs likely associated with a different susceptibility to ZEN inhibition, proofing the possible existence of a certain degree of inter-individual variability to ZEN action. Then, it has been also calculated the inhibitory potential of αZEL toward those aromatase variants (i.e. T310I and T310S) which showed an expected diverse (but not null) inhibition by ZEN compared to WT. This could estimate whether SNV may also affect the susceptibility to αZEL. Such variants have been rationally prioritized for future investigations and the implications of these findings to the current understanding of ZEN toxicology have been also discussed.

2. Materials and methods

2.1. Data source and management

2.1.1. Retrieval of aromatase variants

All the human aromatase (UniProt code P11511) SNVs were retrieved from the "Variant viewer" section of the UniProt database (www.uniprot.org) (Bateman et al. 2023) which listed 434 SNVs at the time of analysis (last database access 25th September 2023). However, the analysis focused on those at the ligand binding pocket (15 SNVs) being most likely to influence the interaction of ZEN. The visual inspection of the 3D structure of human aromatase allowed for the definition of such a subset of SNVs (see below) with the following carried forth the analysis: A306T, D309G, D309N, F221S, M374I, M374L, M374T, R115Q, S478F, T310A, T310I, T310S, V370A, V370M and V370F.

2.1.2. Retrieval of protein and ligands structures

The list of molecules under analysis included ZEN, αZEL, testosterone (TES) and naringenin (NAR) with the latter two taken as reference compounds, and formestane. Their 3D structures were retrieved from PubChem (https://pubchem.ncbi.nlm.nih.gov) (Kim et al. 2023) in the Structure Data File (.sdf) format (CID: 5281576, 5284645, 6013, 439246 and 11273 respectively).

The 3D model of human WT aromatase was derived from the crystallographic structure stored on the Protein Data Bank (PDB; https://www.rcsb.org; last database access 24th July 2023) (Berman et al. 2000) with PDB code 3S79 (Ghosh et al. 2012). This structure was also used to derive the 3D model for the 15 aromatase variants listed above since their crystallographic structure was not available at the time of analysis (see below).

2.1.3. Protein model preparation

The WT 3D structure of human aromatase (PDB code 3S79) (Ghosh et al. 2012) was processed with UCSF Chimera software (version 1.16) (Pettersen et al. 2004) removing water and the co-crystallized ligand and adding hydrogens, in agreement with previous work. The 3D structure of aromatase variants was generated processing the WT structure with Chimera (version 1.16) (Pettersen et al. 2004), replacing selected amino acids using the Structure Editing/Rotamer tool and choosing the rotamer with the highest computed probability to occur when multiple rotamers were computed, in agreement with previous studies (Louisse et al. 2022).

2.2. Docking Simulations

Docking simulations were performed to provide a plausible binding architecture for each molecule under analysis within the aromatase binding site and to predict the effects of different SNVs on the interaction between ZEN and aromatase.

Docking simulations were performed with the GOLD software (version 2021), using the internal GOLDScore scoring function, as already succeeded to calculate the effect of aminoacidic substitutions to the protein-ligand binding (Pedroni et al. 2023a; Pedroni et al. 2023b). The binding site was set within a 5 Å radius sphere around the centroid of the co-crystallized ligand binding site. A semi-flexible docking protocol was applied while allowing protein's polar hydrogens free to rotate and considering ligands fully flexible.

The Root Mean Square Deviation (RMSD) analysis between the calculated and the crystallographic pose of TES was performed with DockRMSD webserver (version 1.1; https://zhanggroup.org/DockRMSD) (Bell and Zhang, 2019) and considering non hydrogen atoms only.

2.3. Molecular Dynamics Simulations

Molecular dynamics (MD) simulations were performed through GROMACS (version 2021.4) (Abraham et al. 2015) to monitor the geometrical stability of the complex and ligand orientation.

All the ligands were processed and parametrised with the SwissParam tool (https://ww.swissparam.ch) (Zoete et al. 2011) and the whole system was parametrised with the CHARMM27 all-atom force field (Brooks et al. 2009). The hydrogen database was modified according to previous works (Dorne et al. 2022; Panneerselvam et al. 2015; Pedroni et al. 2023a; Zhang et al. 2012) to properly parameterise the heme group. The input complex structures were solvated with SPCE water in a dodecahedron periodic boundary condition and neutralized adding Na^+ and Cl^- as counter ions. Before running MD simulations, each system underwent an energetical minimization to both avoid steric clashes and correct improper geometries using the steepest algorithm with a maximum of 5000 steps. Then, each system underwent isothermal (300 K; coupling time of 2 ps) and isobaric (1 bar; coupling time of 2 ps) 100 ps simulations before undergoing 40 ns long MD simulations (300 K with a coupling time of 0.1 ps and 1 bar with a coupling time of 2 ps).

2.4. Statistical analysis

The statistical analysis to compare SNVs and WT using the mean RMSDs of ligands and/or the average interatomic distances between reacting atom and heme's iron was performed with SPSS IBM (v. 27.0, SPSS Inc., Chicago, IL, USA). For each complex, 8000 frames were considered, expressed as means ± standard deviation (SD) and pairwise compared to the WT using t test ($\alpha = 0.05$).

3. Results and Discussion

The work aimed at assessing whether SNVs of aromatase (CYP19A1) occurring among the human population may affect its susceptibility of being inhibited by ZEN. The investigation targeted a selection made from the 434 aromatase SNVs recorded in the UniProt database (www.uniprot.org) (Bateman et al. 2023) at the time of analysis (last database access 25th September 2023) to make the study technically feasible. Specifically, this investigation targeted the substitutions of those amino acids who surrounded the ligand binding site, assuming they are most likely to have an impact on the aromatase-ZEN interaction, which were 15 at the time of analysis: A306T, D309G, D309N, F221S, M374I, M374L, M374T, R115Q, S478F, T310A, T310I, T310S, V370A, V370M and V373F (Fig. 2A) www.uniprot.org

3.1. Assessment of procedural performances

The workflow presented here, which is based on the integrated use of docking simulations and MD, already proofed its efficacy to reliably estimate the effect mutations may have on the capability of protein to recruit ligands (Dorne et al. 2022; Louisse et al. 2022). However, a fit-for-purpose validation was done prior to test whether aromatase SNVs may have a diverse susceptibility to ZEN inhibition.

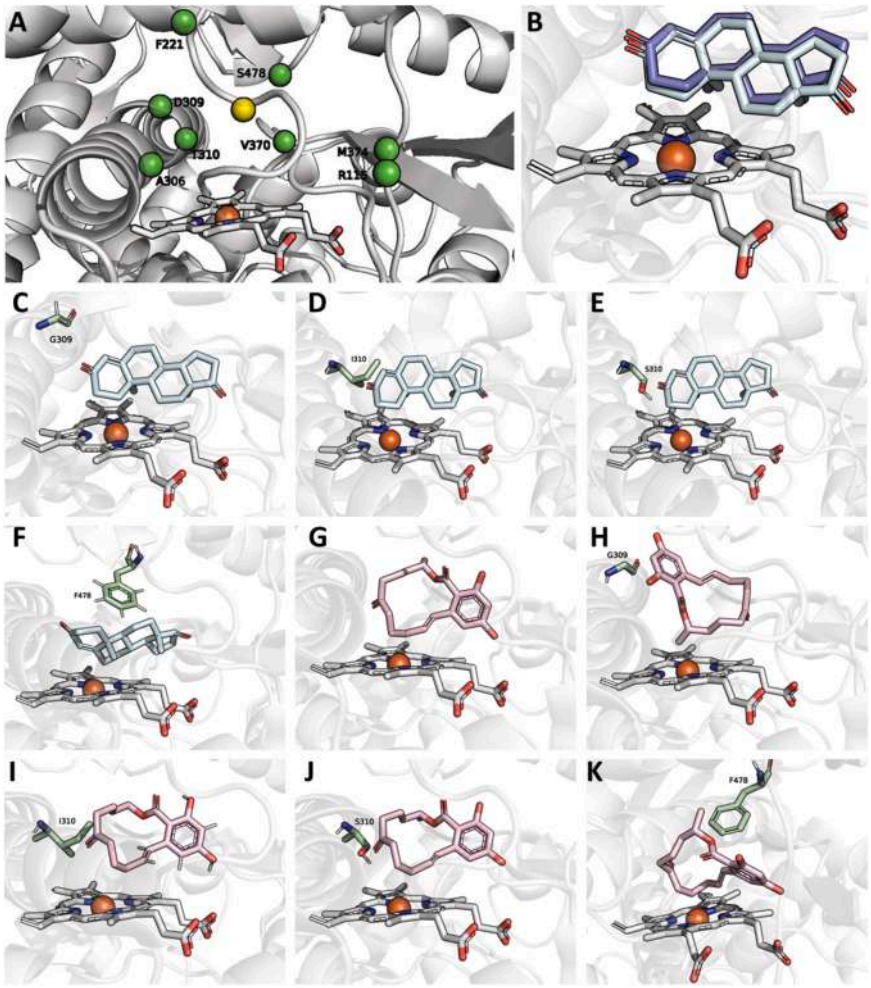

Fig. 2. Protein binding site and docking poses of TES (pale cyan sticks) and ZEN (pale pink sticks) in WT and in a selection of variants. Heme is represented as white sticks while the protein is represented as transparent white cartoon. The mutated residue in each variant is represented as pale green sticks. **A**. Close-up of the protein binding site. The yellow sphere represents the centroid set for the docking simulation while the green spheres indicate the positions of residues mutated in the considered variants. **B**. Close-up of the TES binding pose obtained via docking simulation (pale cyan sticks) overlapped to the crystallographic pose of TES (purple sticks; PDB ID 3S79). **C**. TES docking pose in D309G. **D**. TES docking pose in T310I. **E**. TES docking pose in T310S. **F**. TES docking pose in S478F. **G**. ZEN docking pose in WT. **H**. ZEN docking pose in D309G. **I**. ZEN docking pose in T310I. **J**. ZEN docking pose in T310S. **K**. ZEN docking pose in S478F.

In agreement with previous studies, the procedural performances were assessed following a multi-tier approach (Dellafiora et al. 2022; Louisse et al. 2022). Firstly, the capability to reproduce the binding architecture of TES, taken as reference for aromatase ligands, was checked comparing its calculated and crystallographic poses. As shown in Fig. 2B, the docking pose was very similar to the crystallographic one with a RMSD value of 0.345 Å, supporting the model reliability to calculate meaningful binding architectures. Afterward, the procedure has been challenged using data from the literature to prove its capability to provide geometrical rationales which may effectively estimate the effects of mutations on aromatase activity and susceptibility to inhibition.

To do so, the variants V370M, D309N and T310S, taken as reference being previously assessed for activity and susceptibility to inhibition (Kao et al. 1998; Lo et al. 2013; Ludwig et al. 1998), were analysed combining data from docking and MD simulations. Specifically, it was monitored the geometrical stability of complexes over time using the RMSD of ligands, proteins and ligands trajectories, and monitoring the number of protein-ligand hydrogen bonds over time, in agreement with previous studies (Dorne et al. 2022; Zhao et al. 2021).

V370M and D309N have been previously described as inactive aromatase variants (Kao et al. 1998; Lo et al. 2013; Ludwig et al. 1998), while T310S has been described active though more susceptible of being inhibited by NAR compared to the WT enzyme (Kao et al. 1998). Germane to the mechanism of catalysis, aromatase acts turning the A ring of substrates like TES into an aromatic ring through methyl oxidation resulting in the elimination of the methyl group (Di Nardo et al. 2015). To do so and according to previous studies (Dorne et al. 2022), the methyl group undergoing the reaction must be closely and stably oriented toward the catalytic core of the enzyme, namely the heme's iron atom (Fig. 3A).

3.1.1. *Inactive variants (V370M, D309N)*

Concerning V370M, in line with this evidence, TES has been docked into the WT aromatase and in the V370M variant. Of note, docking scores may correlate with the capability of ligands to fit the protein pockets and positive scores typically indicate a good fitting (the higher the score, the better the fitting of ligands into the pocket; https://www.ccdc.cam.ac.uk/). In this respect, the docking scores TES recorded into the WT aromatase and the V370M were 63.15 and –16.51 units, respectively. The negative score TES recorded in the V370M variant pointed to the strong impairing effects this substitution had in terms of TES-pocket fitting. Then, both complexes were further analysed with MD simulations. Specifically, the interatomic distance between the carbon of the methyl group undergoing the reaction and the heme's iron atom was measured over time comparing those observed for the WT

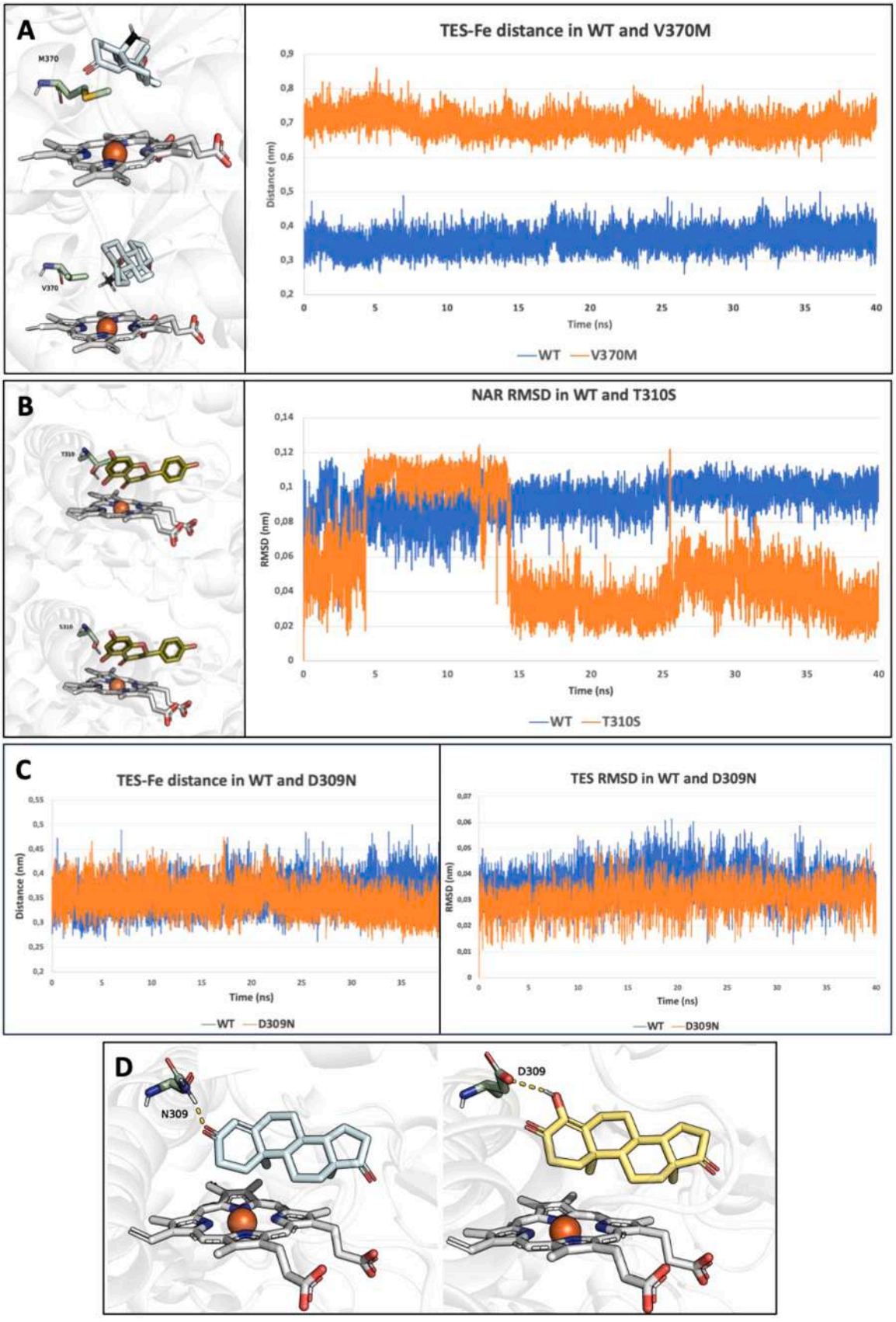

(caption on next page)

Fig. 3. Model validation. Protein is reported as transparent white cartoon while heme in white sticks. The average distances between the atom undergoing reaction and heme's iron atom ± SD are reported between brackets. **A**. Comparison between TES-V370M and TES-WT complex. TES is represented as pale cyan sticks with the methyl group undergoing the reaction as black sticks. On the top-left, TES docking pose in the SNV V370M while below TES docking pose in the WT. The residues V370 and M370 are reported as pale green sticks. On the right, interatomic distances between TES's atom undergoing reaction and heme's iron within WT (blue; 0.359 ± 0.032 nm) and in V370M (orange; 0.699 ± 0.031 nm). **B**. Comparison between NAR-T310S and NAR-WT complex. NAR is represented as green olive sticks. On the top-left, NAR docking pose in the WT while below NAR docking pose in the SNV T310S. The residues T310 and S310 are reported as pale green sticks. On the right, NAR RMSD within WT (blue; 0.092 ± 0.011 nm) and T310S (orange; 0.057 ± 0.031 nm). **C**. On the left, interatomic distances between TES's atom undergoing reaction and heme's iron within WT (blue; 0.359 ± 0.032 nm) and D309N (orange; 0.348 ± 0.030 nm). On the right, TES RMSD within WT (blue; 0.036 ± 0.006 nm) and D309N (orange; 0.030 ± 0.005 nm) **D**. On the left, TES (pale cyan sticks) docking pose in the D309N SNV. The dashed yellow lines represent the hydrogen bond between N309 (pale green sticks) and TES. On the right, formestane (pale yellow sticks) docking pose within WT. The dashed yellow lines represent the hydrogen bond between D309 (pale green sticks) and formestane.

aromatase with those of the inactive V370M variant. As shown in Fig. 3A, docking analysis revealed that the V370M substitution was responsible for a diverse arrangement of TES compared to the WT enzyme where the methyl group undergoing the reaction was not properly oriented as saw in the WT complex. Moreover, MD revealed that the distance between the methyl group in V370M is significantly ($p < 0.001$) farer to the heme's iron over time compared to the WT enzyme (0.699 ± 0.031 and 0.359 ± 0.032 nm, respectively). In line with previous studies (Dorne et al. 2022), this evidence confirmed geometrical rationales such as the arrangement at the binding site and the distance of the atom undergoing the reaction to the heme's iron measured over time as meaningful parameters to estimate the effects of mutations on aromatase capability to turn substrates into products. Besides, to the best of our knowledge, these results provide a first convincing mechanistic explanation for the inactivity of V370M variant. Specifically, our findings suggest that mutations able to "shield" the heme's iron from the atom undergoing the reaction are likely to reduce the enzyme activity. Indeed, the dynamics of interaction observed in V370M suggest that this hindrance possibly occurs when the substitution involves bulky amino acids, thereby preventing the atom undergoing the reaction to get close to the enzyme's catalytic core.

Concerning D309N, at a first instance the docking results and the interaction of TES monitored over time with MD simulations were apparently contradictory to the reported inactivity of this variant. Indeed, the docking scores TES recorded in the WT aromatase and in the D309N variant were comparable (63.15 and 63.99 units, respectively) as well as the complex with the variant was barely comparable to the WT in terms of interatomic distance between the TES reacting atom and heme's iron (0.348 ± 0.030 nm and 0.359 ± 0.032, respectively), and ligand RMSD trends and average values (the latter were 0.030 ± 0.005 and 0.036 ± 0.006, respectively) (Fig. 3C). This evidence pointed to the substantial capability of TES to interact with the D309N variant. Interestingly, a deeper analysis of aromatase pharmacodynamics provided a convincing explanation of the reason why D309N may result inactive although TES can stably persist at the catalytic site, as per our outcome. Indeed, TES showed in D309N a stably higher number of hydrogen bonds compared to the WT, with an additional bond between the keto group in position 3 and the N309 polar side chain (Fig. 3D). Interestingly, this evidence could explain the mechanisms underpinning the inactivity of D309N variant. Indeed, the interpretative line that an additional hydrogen bond may result in enzyme inactivity, i.e. incapability to turn the substrate TES into products, agrees with the pharmacodynamic of the aromatase inhibitor formestane. Formestane has a steroidal scaffold differing from aromatase substrates uniquely for an additional hydroxyl group in position 4 which has been described forming a hydrogen bond with the side chain of D309 (Di Nardo et al. 2015; Murthy et al. 2005), as also shown in our docking studies (GOLDScore 63.21 units; Fig. 3D). The interaction with the D309 residue is critical for the inhibitory mechanisms of formestane being involved in the electron transfer, which is altered to the point of enzyme inhibition when is engaged in hydrogen bonds (Martin et al. 2016; Murthy et al. 2005). Therefore, although the D>N substitution is likely to have an inherently altered electron transfer capacity, the additional hydrogen bond described in this study is also compatible with a disrupting action in electron transfer and could provide a mechanistic explanation for inactivity of D309N variant.

Of note, the outcome of D309N and V370M, beside pointing to the procedural reliability to properly estimate the effects of mutations on aromatase activity, may help shedding light on the mechanics of aromatase deficiency, a possibly severe clinical condition. Indeed, a more informed mechanistic understanding of aromatase SNVs provides potentially relevant pieces of information to integrate its current clinical/pharmacological understanding and plan future dedicated studies.

3.1.2. *Susceptible variant (T310S)*

Germane to NAR, it is a flavonoid reported as a phytoestrogen responsible for aromatase inhibition while the T310S variant is a functional variant more susceptible to NAR inhibition compared to the WT enzyme (Lephart, 2015). Also in this case, NAR has been docked into the WT aromatase and into the T310S variant (Fig. 3B). The GOLDScore of NAR into the WT aromatase and the T310S variant were 55.47 and 57.73 units, respectively. Docking studies revealed that NAR was comparably arranged at the ligand binding site with minor differences between the WT enzyme and its variant. However, the 4% higher score observed for NAR in complex with the T310S variant could point to the better fitting compared to the WT enzyme. Then, the geometrical stability of NAR in the WT enzyme and its T310S variant has been monitored over time through MD simulations. As shown in Fig. 3B, MD simulations revealed that the interaction of NAR with the T310S variant was significantly more stable than that with the WT enzyme with average RMSD significantly ($p < 0.001$) lower (0.057 ± 0.031 nm in T310S; 0.092 ± 0.011 nm in WT). Of note, as discussed elsewhere (Zhao et al. 2021), an enhanced geometrical stability like that described here for NAR is compatible with an increased capability of ligands to persist at the ligand binding site and, in case of enzymes, this can correlate with a higher inhibitory capacity, in line with the experimental evidence of T310S variant inhibition by NAR (Kao et al. 1998).

Overall, these outcomes confirmed the geometrical rationales provided by the integrated use of docking and MD simulations described above, including the hydrogen bond network monitored over time, as meaningful to study the activity and the susceptibility of being inhibited of aromatase variants. Therefore, the *in silico* workflow presented here turned out to be reliable to estimate the effects of aromatase variants on its susceptibility of being inhibited by ZEN.

3.2. *Study of interaction between ZEN, αZEL and aromatase variants*

Once the procedural performances have been validated (see Section 3.1), the interaction of ZEN with the following variants was investigated: A306T, D309G, F221S, M374I, M374L, M374T, R115Q, S478F, T310A, T310I, T310S, V370A, and V373F. The interaction of ZEN with V370M and D309N variants was not calculated instead being these variants inactive. Furthermore, it has been calculated the capability of αZEL to inhibit WT and those predicted active variants with a theoretically diverse sensitivity of being inhibited by ZEN with respect to the WT.

3.2.1. *Interaction between ZEN and aromatase variants*

The interaction of ZEN has been calculated along with that of TES in

all the variants listed above via docking simulations to make a short list of complexes to investigate further with MD simulations. The selection criterion was based on the docking score assignment and respective variations observed in the aromatase variants compared to WT, assuming that the variations magnitude may reflect the impact of amino acid substitution in the capability to bind ZEN, in agreement with previous studies (Dorne et al. 2022; Louisse et al. 2022). Specifically, docking scores may correlate with the capability of ligands to fit the protein pocket (i.e. the higher the score, the better the fitting into the pocket), as previously described (Ji et al. 2020; Louisse et al. 2022). Therefore, all the 13 collected variants were analysed through molecular docking and the docking scores compared to that recorded for the WT enzyme. Then, those complexes having mutations expected to be most effective (scores variations above 10%; threshold arbitrarily set, namely S478F, D309G and T310I) have been further studied with MD simulations (see Table 1; Fig. 2B-K). The T310S was also analysed although the % variation was below 10% as it was previously described having a diverse susceptibility to inhibition (Kao et al. 1998).

T310S. As for V370M, T310S was used also to assess model performances as it is more susceptible to NAR inhibition, as described in Section 3.1. Concerning the interaction with ZEN (Fig. 2J), docking results revealed a score slightly higher (+4.4%) compared to the WT. This might point to a better fitting into the enzyme pocket possibly resulting in an enhanced inhibitory activity. The ligand-T310S complex stability analysed thorough MD simulations highlighted a WT-like behaviour when in complex with TES while ZEN resulted as more stable in T310S than in WT (Fig. 4A). Indeed, the T > S substitution likely leads to an enlargement of the pocket volume, due to the lower dimension of serine side chain compared to threonine, which resulted in a better accommodation of ZEN. Based on these findings, T310S could be associated with a possible increased susceptibility towards ZEN inhibition. It must be noted that the xenoestrogenic potential of ZEN depends - though is not limited to - on the concerted activation of ERs and inhibition of aromatase. Therefore, based on this outcome, it cannot be excluded that individuals bearing this variant might have a diverse endocrine disruption when exposed to ZEN compared to those homozygotes for the WT enzyme. Specifically, in subjects bearing the T310S variant, ZEN might have a higher depleting activity of estrogens production, the effects of which at the level of hormones homeostasis and related pathogenesis are worth of future investigations. Despite this SNV recorded a low frequency among human population (minor allele frequency < 0.0006; as per UniProt last access 26th September 2023), its occurrence, expression and frequency should be deeply investigated as fundamental for its relevance to ZEN toxicity in living organisms.

Table 1
Docking results for ZEN and TES into WT aromatase and a selection of its variants.

Aromatase	Ligand	GOLDScore	% variation to the WT[1]
Wild-type	TES	63.15	—
	ZEN	45.92	—
	αZEL	36.55	—
A306T	TES	64.45	-2.1
	ZEN	41.65	9.3
D309G	TES	60.96	3.5
	ZEN	53.58	-16.7
F221S	TES	61.96	1.9
	ZEN	48.68	-6.0
M374I	TES	61.6	2.5
	ZEN	46.16	-0.5
M374L	TES	63.05	0.2
	ZEN	45.78	0.3
M374T	TES	62.86	0.5
	ZEN	45.92	0.0
R115Q	TES	60.54	4.1
	ZEN	45.60	0.7
S478F	TES	19.98	68.4
	ZEN	-35.25	—
T310A	TES	60.68	3.9
	ZEN	45.97	-0.1
T310I	TES	39.05	38.2
	ZEN	31.90	30.5
	αZEL	31.40	14.1
V370A	TES	59.12	6.4
	ZEN	43.35	5.6
V373F	TES	65.06	-3.0
	ZEN	48.04	-4.6
T310S[2]	TES	61.20	3.1
	ZEN	47.92	-4.4
	αZEL	44.30	-21.2

Note: [1] the sign "-" indicates scores higher compared to the those observed into the wild-type enzyme. [2] The complex with T310S was analysed through MD simulations although the % variation was below 10% because previous evidence reported the effects of such substitution in terms of susceptibility to inhibition (Kao et al., 1998). Complexes with a % variation above 10% were analysed through MD simulations and are indicated in bold.

S478F. As shown in Fig. 2F, the S>F substitution caused an improper arrangement of TES with respect to the WT where the interatomic distances between the atom undergoing the reaction and the heme's iron are kept significantly ($p < 0.001$) lower (average distance of 0.359 ± 0.032 and 0.455 ± 0.057 nm in WT and S478F, respectively) (Fig. 5A). Therefore, this aromatase SNV has been considered not functional for the reason already discussed for V370M. Therefore, ZEN has not been calculated via MD simulation accordingly, although the negative docking score recorded pointed to the substantial incapability of ZEN to fit in. On this basis, S478F might be associated to aromatase deficiency and although it has been found having a low frequency among human population (minor allele frequency of 0.0002; as per UniProt, last access 26th September 2023) it is worthy of further analysis to characterize its occurrence, expression and activity.

D309G. This SNV recorded for TES a docking score comparable to WT, while it obtained a 16.7% score increase with ZEN, pointing to a possible higher susceptibility. However, MD simulations showed ZEN as less stable in D309G than in WT (Fig. 5B), indicating a probable reduced ZEN inhibitory activity, while TES had a comparable behaviour. Of note, the D309 is a crucial residue for the electron transfer (see Section 3.1), and considering the different physico-chemical properties of glycine with respect to glutamate, the D309G substitution might be related to aromatase deficiency. Moving to the SNV frequency, it is low (minor allele frequency < 0.00008; as per UniProt, last access 26th September 2023) but a better characterization of its occurrence, expression and activity should be carried out anyway.

T310I. The T > I substitution led to a WT-like arrangement of TES (Fig. 2D) and ZEN (Fig. 2I). However, the former recorded a 30.5% docking score decrease while the latter a 40.1% decrease possibly due to the different polarity of isoleucine and threonine. The MD simulations interestingly led to similar results compared to the WT, indeed both TES and ZEN recorded trends similar to the respective WT complexes (Fig. 4B). Nevertheless, seen the drop in the docking score and the substitution of a residue with different physico-chemical properties, T310I was considered as less capable of binding both the natural substrates and ZEN, though its activity and inhibition would deserve a further quantitative assessment. Regarding its frequency, this is low (minor allele frequency < 0.00006; as per UniProt, last access 26th September 2023) but, as for the others considered SNVs, its occurrence, expression and activity should be furtherly analysed as fundamental for its relevance to ZEN toxicity in living organisms.

3.3. Interaction between αZEL, T310S and T310I aromatase variants

Previous evidence described αZAL, a close analogue of αZEL , as able to inhibit aromatase though with a lower efficacy compared to ZEN (Wang et al. 2014), suggesting a certain degree of inhibitory potential for αZEL as well. Moreover, αZEL is a more potent agonist of ER compared to ZEN (Chain, 2014). The stronger activation of ERs and the expected weaker inhibition of aromatase (hypothesized based on αZAL data) are likely part of the mechanisms underpinning the stronger

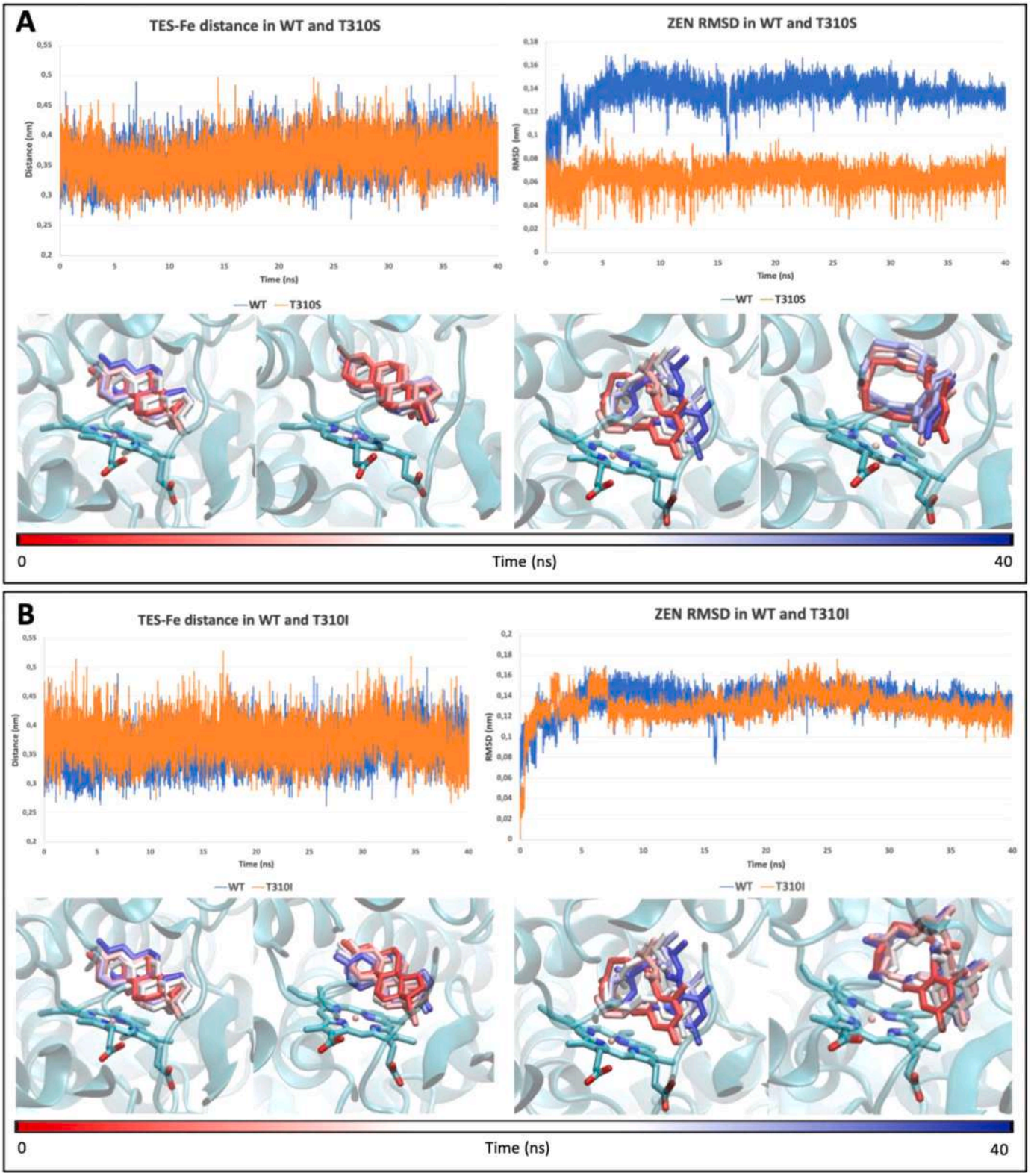

Fig. 4. MD results on T310 variants compared to WT. The average distances between the atom undergoing reaction and heme's iron atom ± SD are reported between brackets. **A**. On the top-left, interatomic distances between TES's atom undergoing reaction and heme's iron within WT (blue; 0.359 ± 0.032 nm) and T310S (orange; 0.364 ± 0.033 nm). On the bottom-left, time-step representation (from red, 0 ns, to blue, 40 ns) of the trajectories of TES within WT and T310S. On the top-right, ZEN RMSD within WT (blue; 0.136 ± 0.013 nm) and T310S (orange; 0.065 ± 0.009 nm). On the bottom-right, time-step representation (from red, 0 ns, to blue, 40 ns) of the trajectories of ZEN within WT and T310S. **B**. On the top-left, interatomic distances between TES's atom undergoing reaction and heme's iron within WT (blue; 0.359 ± 0.032 nm) and T310I (orange; 0.376 ± 0.033 nm). On the bottom-left, time-step representation (from red, 0 ns, to blue, 40 ns) of the trajectories of TES within WT and T310I. On the top-right, ZEN RMSD within WT (blue; 0.136 ± 0.013 nm) and T310I (orange; 0.130 ± 0.015 nm). On the bottom-right, time-step representation (from red, 0 ns, to blue, 40 ns) of the trajectories of ZEN within WT and T310I.

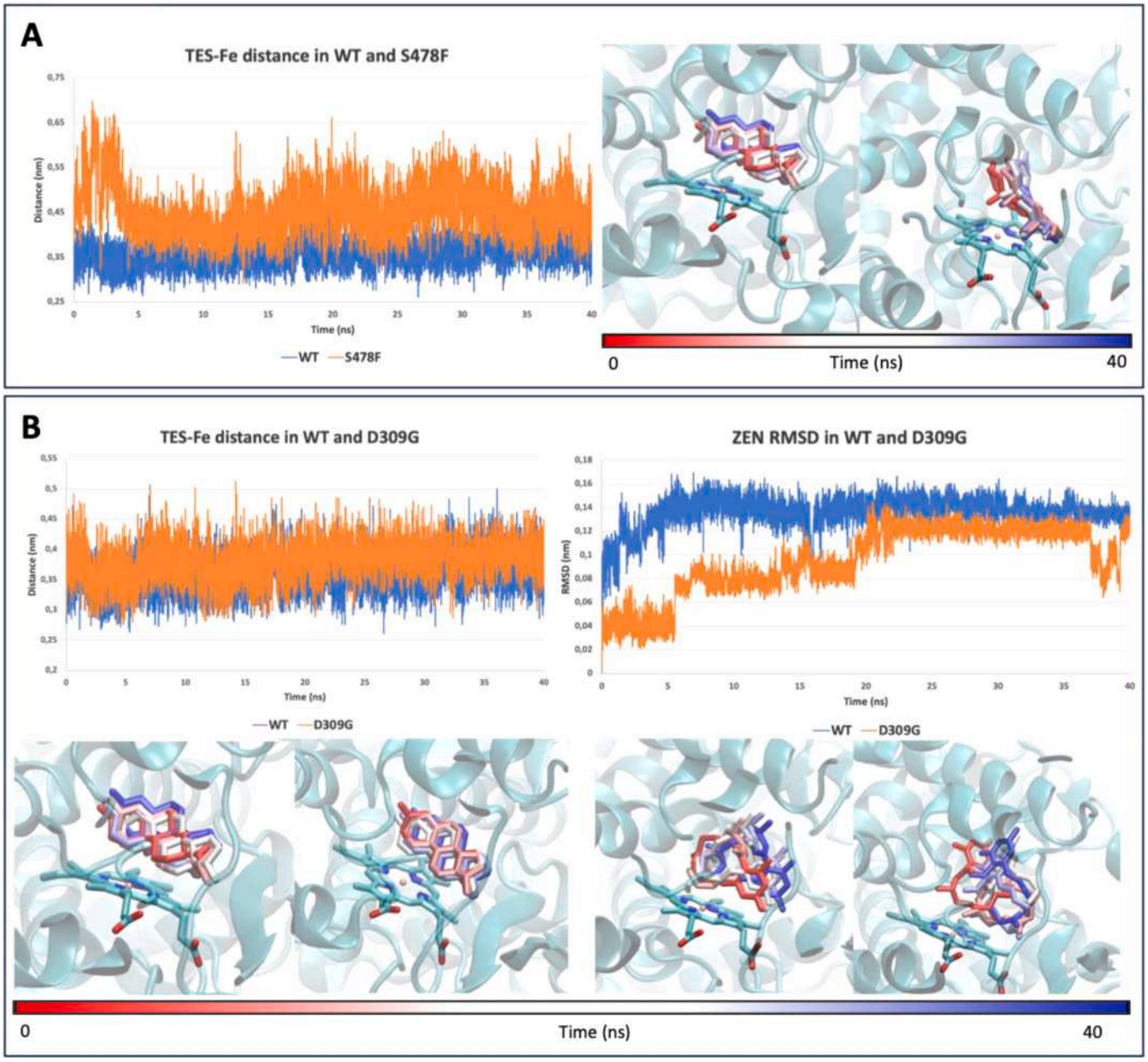

Fig. 5. MD results on S478F and D309G compared to WT. **A**. On the left, interatomic distances between TES's atom undergoing reaction and heme's iron within WT (blue; average value ± SD of 0.359 ± 0.032 nm) and S478F (orange; average value ± SD of 0.455 ± 0.057 nm). On the right, time-step representation (from red, 0 ns, to blue, 40 ns) of the trajectories of TES within WT and S478F. **B**. On the top-left, interatomic distances between TES's atom undergoing reaction and heme's iron within WT (blue; average value ± SD of 0.359 ± 0.032 nm) and D309G (orange; average value ± SD of 0.381 ± 0.032 nm). On the bottom-left, time-step representation (from red, 0 ns, to blue, 40 ns) of the trajectories of TES within WT and D309G. On the top-right, ZEN RMSD within WT (blue; average value ± SD of 0.136 ± 0.013 nm) and D309G (orange; average value ± SD of 0.095 ± 0.029 nm). On the bottom-right, time-step representation (from red, 0 ns, to blue, 40 ns) of the trajectories of ZEN within WT and D309G.

estrogenic insult αZEL may have in certain systems compared to ZEN. Therefore, studying whether SNV may also vary the susceptibility of aromatase to αZEL inhibition is important to better understand the general mechanics of ZEN estrogenicity. This is particularly significant since αZEL is one of the most abundant ZEN phase I metabolite in humans. The analysis was focused on WT aromatase an on those variants who gave evidence of a predicted diverse though not null susceptibility to ZEN compared to the WT (i.e. T310I and T310S).

As shown in Table 1, αZEL recorded a lower score within the WT compared to ZEN (36.55 and 45.92 units, respectively), in line with the weaker inhibitory activity described previously for its structural analogue αZAL (Wang et al. 2014). This confirmed that αZEL may eventually have a reduced inhibitory activity, as hypothesized above. The score decrease compared to ZEN may be due to the slightly diverse arrangement αZEL showed into the pocket (Fig. 6). Moreover, αZEL recorded a 21.2% higher and 14.1% lower score compared to the WT within T310S and T310I, respectively, suggesting that αZEL may preferentially interact and inhibit T310S than the WT, as described for ZEN above. The analysis of trajectories revealed that αZEL could stably stay at the ligand binding site of WT, T310S and T310I (Fig. 6). However, the RMSD trend observed within T310S was more stable compared to that within WT. Concerning T310I, αZEL showed a RMSD trend like that

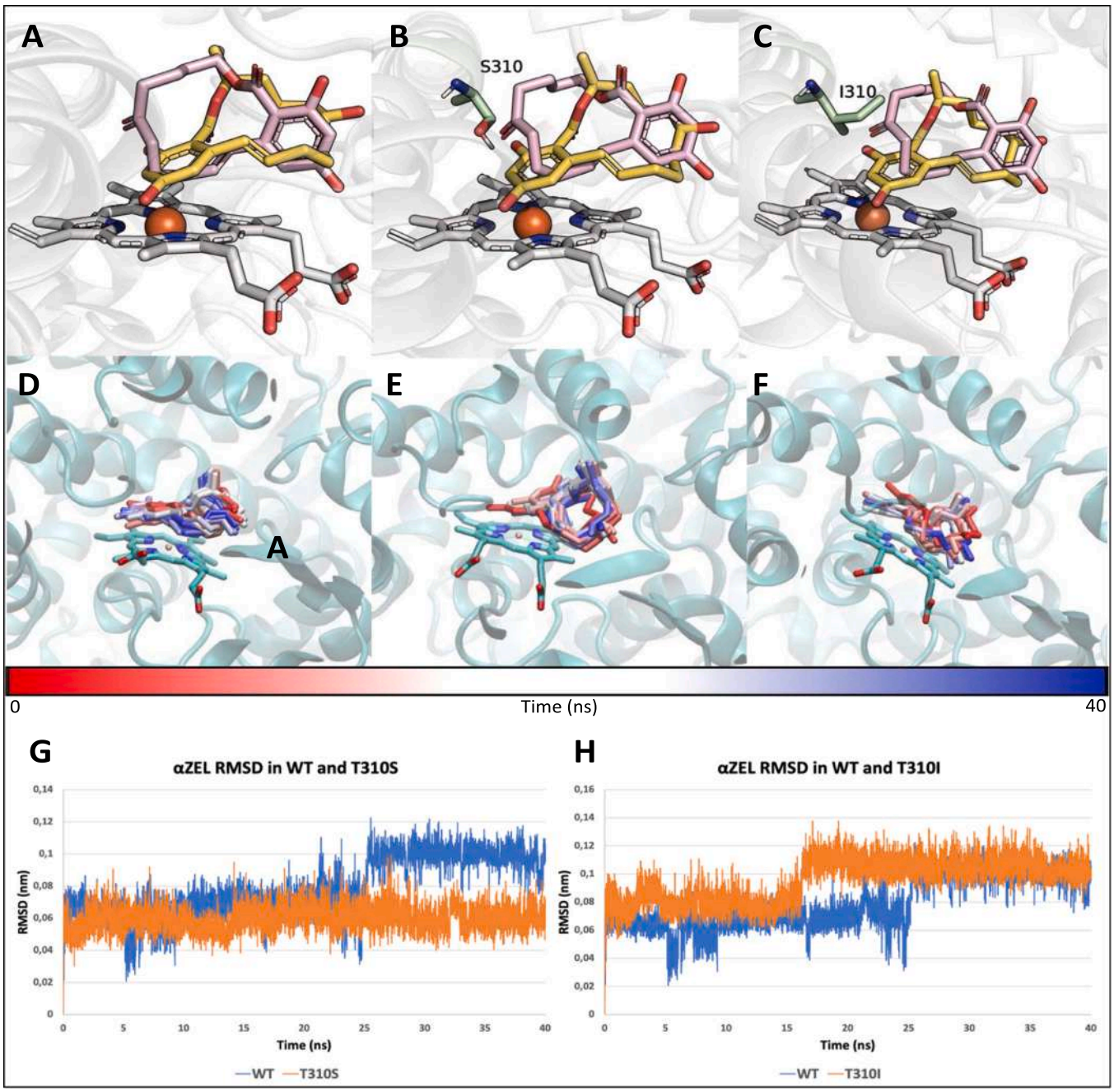

Fig. 6. Molecular docking and MD simulations results of αZEL within T310S and T310I compared to WT. **A.** Docking pose superimposition of ZEN (pink sticks) and αZEL (yellow sticks) within WT. **B.** Docking pose superimposition of ZEN (pink sticks) and αZEL (yellow sticks) within T310S. **C.** Docking pose superimposition of ZEN (pink sticks) and αZEL (yellow sticks) within T310I. **D.** Time-step representation (from red, 0 ns, to blue, 40 ns) of the trajectories of αZEL within WT. **E.** Time-step representation (from red, 0 ns, to blue, 40 ns) of the trajectories of αZEL within T310S. **F.** Time-step representation (from red, 0 ns, to blue, 40 ns) of the trajectories of αZEL within T310I. **G.** αZEL RMSD within WT (blue; average value ± SD of 0.078 ± 0.018 nm) and T310S (orange; average value ± SD of 0.059 ± 0.008 nm). **H.** αZEL RMSD within WT (blue; average value ± SD of 0.078 ± 0.018 nm) and T310I (orange; average value ± SD of 0.095 ± 0.016 nm).

observed within the WT. Therefore, in line with the interpretation made for ZEN, these outcomes could suggest that T310S might be more susceptible to αZEL inhibition compared to the WT. Importantly, this and the associated reduced production of estrogens need further dedicated investigations to prove whether T310S bearing subjects may "benefit" of a mitigated estrogenic insult when exposed to αZEL or ZEN – considering ZEN prominent conversion to αZEL. The verification of such hypothesis is crucial considering that the estrogenic effect of ZEN and metabolites, including αZEL, results from the concerted activation of ER and aromatase inhibition, as discussed above.

4. Conclusions

This work dealt with the analysis of aromatase SNVs with respect to their susceptibility to be inhibited by ZEN and αZEL. The analysis is framed into the context of ZEN toxicodynamics and its variability among the human population. These investigations are fundamental to improve the current understanding of ZEN toxicology, also paving the way for a more informed study of the ZEN-dependent pathogenic potential at an individual level. Our work coped with the aromatase SNVs available at the time of analysis focusing on a set of variants that have been thoroughly investigated using a validated and well-consolidated molecular

modelling approach. The S478F has been described likely having a severely impaired capacity to receive substrates, suggesting its reduced/null catalytic activity and possible involvement in aromatase deficiency. The possible association to a reduced/null activity has been also described for D309G, for which an impairing effect of the D>G substitution has been postulated based on the key role of D309 for catalysis. The T310I was calculated having a minor role to impair the capability to recruit and interact with TES and ZEN. This might suggest a susceptibility of being inhibited by ZEN comparable to the WT, though expression and activity should be further analyzed for a better characterization of this variant. Finally, the T310S variant was found more susceptible to ZEN inhibition, in line with the effect previously described for NAR, while keeping its activity to convert endogenous substrates (Kao et al. 1998). This suggested that those individuals bearing this variant might be diversly affected by ZEN considering the postulated reduced capability of being inhibited and the comparable activity to convert endogenous substrates. Concerning αZEL, this study described that it may inhibit aromatase, though with an expected lower potency than ZEN, like its close structural analogue αZAL. Moreover, in line with the interpretation made for ZEN, T310S may have an enhanced susceptibility of being inhibited compared to the WT. Taken together the results collected for ZEN and αZEL highlighted that the aromatase inhibitory capacity of ZEN must be investigated along with that of its congeners and metabolites, also with respect to their relative production in living organisms and respective inhibitory activity towards aromatase SNVs. This should be carefully evaluated toward a better understanding and assessment of ZEN and congeners as a group of toxicants rather than single substances, as outlined by EFSA (Alexander et al. 2016).

As a general comment, the present work was meant to prioritize SNVs for further analysis toward a better comprehension of ZEN toxicity among the human population. Therefore, this work proposed for further dedicated investigations T310S for the possible increased susceptibility to ZEN and αZEL inhibition, and D309N and S478F for the suspected loss of function. Also, it provided a mechanistic rationale explaining, at least in part, the inactivity of V370M and D309N variants, concurring to improve the basic understanding of their association to aromatase deficiency in humans.

CRediT authorship contribution statement

Dellafiora Luca: Conceptualization, Data curation, Formal analysis, Funding acquisition, Investigation, Methodology, Project administration, Resources, Software, Supervision, Writing – original draft, Writing – review & editing. **Dall'Asta Chiara:** Conceptualization, Writing – review & editing. **Perugino Florinda:** Data curation, Formal analysis, Methodology, Software, Writing – original draft, Writing – review & editing. **Galaverna Gianni:** Conceptualization, Writing – review & editing. **Pedroni Lorenzo:** Data curation, Formal analysis, Investigation, Methodology, Software, Writing – original draft, Writing – review & editing.

Declaration of Competing Interest

The authors declare that they have no known competing financial interests or personal relationships that could have appeared to influence the work reported in this paper.

Data Availability

Data will be made available on request.

Acknowledgments

This research benefits from the HPC (High Performance Computing) facility of the University of Parma, Italy. The author would like to acknowledge Giorgia Tavellin for her contribution in running the analysis.

References

Abraham, M.J., Murtola, T., Schulz, R., Páll, S., Smith, J.C., Hess, B., Lindahl, E., 2015. GROMACS: high performance molecular simulations through multi-level parallelism from laptops to supercomputers. SoftwareX 1–2, 19–25.

Alexander, J., Barregard, L., Bignami, M., Ceccatelli, S., Cottrill, B., Dinovi, M., Edler, L., Grasl-Kraupp, B., Hogstrand, C., Hoogenboom, L., Knutsen, H.K., Nebbia, C.S., Oswald, I., Petersen, A., Rogiers, V.M., Rose, M., Roudot, A.C., Schwerdtle, T., Vleminckx, C., Vollmer, G., Wallace, H., Chain, E.P.C.F., 2016. Appropriateness to set a group health-based guidance value for zearalenone and its modified forms. Efsa J. 14, 4425.

Bateman, A., Martin, M.J., Orchard, S., Magrane, M., Ahmad, S., Alpi, E., Bowler-Barnett, E.H., Britto, R., Cukura, A., Denny, P., Dogan, T., Ebenezer, T., Fan, J., Garmiri, P., Gonzales, L.J.D., Hatton-Ellis, E., Hussein, A., Ignatchenko, A., Insana, G., Ishtiaq, R., Joshi, V., Jyothi, D., Kandasaamy, S., Lock, A., Luciani, A., Lugaric, M., Luo, J., Lussi, Y., MacDougall, A., Madeira, F., Mahmoudy, M., Mishra, A., Moulang, K., Nightingale, A., Pundir, S., Qi, G.Y., Raj, S., Raposo, P., Rice, D.L., Saidi, R., Santos, R., Speretta, E., Stephenson, J., Totoo, P., Turner, E., Tyagi, N., Vasudev, P., Warner, K., Watkins, X., Zellner, H., Bridge, A.J., Aimo, L., Argoud-Puy, G.L., Auchincloss, A.H., Axelsen, K.B., Bansal, P., Baratin, D., Neto, T. M.B., Blatter, M.C., Bolleman, J.T., Boutet, E., Breuza, L., Gil, B.C., Casals-Casas, C., Echioukh, K.C., Coudert, E., Cuche, B., de Castro, E., Estreicher, A., Famiglietti, M.L., Feuermann, M., Gasteiger, E., Gaudet, P., Gehant, S., Gerritsen, V., Gos, A., Gruaz, N., Hulo, C., Hyka-Nouspikel, N., Jungo, F., Kerhornou, A., Le Mercier, P., Lieberherr, D., Masson, P., Morgat, A., Muthukrishnan, V., Paesano, S., Pedruzzi, I., Pilbout, S., Pourcel, L., Poux, S., Pozzato, M., Pruess, M., Redaschi, N., Rivoire, C., Sigrist, C.J.A., Sonesson, K., Arighi, C.N., Armin-ski, L., Chen, C.M., Chen, Y.X., Huang, H.Z., Laiho, K., McGarvey, P., Natale, D.A., Ross, K., Vinayaka, C.R., Wang, Q.H., Wang, Y.Q., Zhang, J., Bye-A-Jee, H., Zaru, R., Sundaram, S., Wu, C.H., UniProt, C., 2023. UniProt: the universal protein knowledgebase in 2023. Nucleic Acids Research 51, pp. D523–D531.

Bell, E.W., Zhang, Y., 2019. DockRMSD: an open-source tool for atom mapping and RMSD calculation of symmetric molecules through graph isomorphism. J. Chemin.-. 11, 40.

Berman, H.M., Westbrook, J., Feng, Z., Gilliland, G., Bhat, T.N., Weissig, H., Shindyalov, I.N., Bourne, P.E., 2000. The protein data bank. Nucleic Acids Res. 28, 235–242.

Brooks, B.R., Brooks, C.L., Mackerell, A.D., Nilsson, L., Petrella, R.J., Roux, B., Won, Y., Archontis, G., Bartels, C., Boresch, S., Caflisch, A., Caves, L., Cui, Q., Dinner, A.R., Feig, M., Fischer, S., Gao, J., Hodoscek, M., Im, W., Kuczera, K., Lazaridis, T., Ma, J., Ovchinnikov, V., Paci, E., Pastor, R.W., Post, C.B., Pu, J.Z., Schaefer, M., Tidor, B., Venable, R.M., Woodcock, H.L., Wu, X., Yang, W., York, D.M., Karplus, M., 2009. CHARMM: the biomolecular simulation program. J. Comput. Chem. 30, 1545–1614.

Catteuw, A., Broekaert, N., De Baere, S., Lauwers, M., Gasthuys, E., Huybrechts, B., Callebaut, A., Ivanova, L., Uhlig, S., De Boevre, M., De Saeger, S., Gehring, R., Devreese, M., Croubels, S., 2019. Insights into in vivo absolute oral bioavailability, biotransformation, and toxicokinetics of zearalenone, alpha-zearalenol, beta-zearalenol, zearalenone-14-glucoside, and zearalenone-14-sulfate in pigs. J. Agric. Food Chem. 67, 3448–3458.

Chain, E.Po.CitF., 2014. Scientific Opinion on the risks for human and animal health related to the presence of modified forms of certain mycotoxins in food and feed. EFSA J. 12, 3916.

Claeys, L., Romano, C., De Ruyck, K., Wilson, H., Fervers, B., Korenjak, M., Zavadil, J., Gunter, M.J., De Saeger, S., De Boevre, M., Huybrechts, I., 2020. Mycotoxin exposure and human cancer risk: A systematic review of epidemiological studies. Compr. Rev. Food Sci. Food Saf. 19, 1449–1464.

De Boevre, M., Jacxsens, L., Lachat, C., Eeckhout, M., Di Mavungu, J.D., Audenaert, K., Maene, P., Haesaert, G., Kolsteren, P., De Meulenaer, B., De Saeger, S., 2013. Human exposure to mycotoxins and their masked forms through cereal-based foods in Belgium. Toxicol. Lett. 218, 281–292.

Dellafiora, L., Magnaghi, F., Galaverna, G., Dall'Asta, C., 2022. A mechanistic investigation on kokumi-active gamma-Glutamyl tripeptides - a computational study to understand molecular basis of their activity and to identify novel potential kokumi-tasting sequences. Food Res. Int. 162, 111932.

Di Nardo, G., Breitner, M., Bandino, A., Ghosh, D., Jennings, G.K., Hackett, J.C., Gilardi, G., 2015. Evidence for an Elevated Aspartate pK(a) in the active site of human aromatase. J. Biol. Chem. 290, 1186–1196.

Dorne, J., Cirlini, M., Louisse, J., Pedroni, L., Galaverna, G., Dellafiora, L., 2022. A computational understanding of inter-individual variability in CYP2D6 activity to investigate the impact of missense mutations on ochratoxin A metabolism. Toxins 14, 207.

EFSA, 2011. Scientific Opinion on the risks for public health related to the presence of zearalenone in food. EFSA J. 9, 2197.

Ekwomadu, T., Mwanza, M., Musekiwa, A., 2022. Mycotoxin-linked mutations and cancer risk: a global health issue. Int. J. Environ. Res. Public Health 19, 7754.

Ghosh, D., Lo, J., Morton, D., Valette, D., Xi, J.L., Griswold, J., Hubbell, S., Egbuta, C., Jiang, W.H., An, J., Davies, H.M.L., 2012. Novel aromatase inhibitors by structure-guided design. J. Med. Chem. 55, 8464–8476.

Gupta, R.C., Doss, R.B., Lall, R., Srivastava, A., Sinha, A., 2022. Chapter 49 - Trichothecenes and zearalenone. In: Gupta, R.C. (Ed.), Reproductive and Developmental Toxicology, Third Edition. Acad. Press, pp. 1003–1016.

IARC, 1993. IARC monographs on the evaluation of carcinogenic risks to humans. IARC Monogr. 56, 599.

Ji, D.W., Xu, M., Udenigwe, C.C., Agyei, D., 2020. Physicochemical characterisation, molecular docking, and drug-likeness evaluation of hypotensive peptides encrypted in flaxseed proteome. Curr. Res. Food Sci. 3, 41–50.
Jing, S.Y., Liu, C.M., Zheng, J., Dong, Z.J., Guo, N., 2022. Toxicity of zearalenone and its nutritional intervention by natural products. Food Funct. 13, 10374–10400.
Kao, Y.C., Zhou, C.B., Sherman, M., Laughton, C.A., Chen, S., 1998. Molecular basis of the inhibition of human aromatase (estrogen synthetase) by flavone and isoflavone phytoestrogens: a site-directed mutagenesis study. Environ. Health Perspect. 106, 85–92.
Katzenellenbogen, J.A., Mayne, C.G., Katzenellenbogen, B.S., Greene, G.L., Chandarlapaty, S., 2018. Structural underpinnings of oestrogen receptor mutations in endocrine therapy resistance. Nat. Rev. Cancer 18, 377–388.
Kim, S., Chen, J., Cheng, T.J., Gindulyte, A., He, J., He, S.Q., Li, Q.L., Shoemaker, B.A., Thiessen, P.A., Yu, B., Zaslavsky, L., Zhang, J., Bolton, E.E., 2023. PubChem 2023 update. Nucleic Acids Res. 51, D1373–D1380.
Knutsen, H.K., Alexander, J., Barregård, L., Bignami, M., Brüschweiler, B., Ceccatelli, S., Cottrill, B., Dinovi, M., Edler, L., Grasl-Kraupp, B., Hogstrand, C., Hoogenboom, L., Nebbia, C.S., Petersen, A., Rose, M., Roudot, A.C., Schwerdtle, T., Vleminckx, C., Vollmer, G., Wallace, H., Dall'Asta, C., Dänicke, S., Eriksen, G.S., Altieri, A., Roldán-Torres, R., Oswald, I.P., Chain, E.P.C.F., 2017. Risks for animal health related to the presence of zearalenone and its modified forms in feed. Efsa J. 15, e04851.
Kowalska, K., Habrowska-Gorczynska, D.E., Piastowska-Ciesielska, A.W., 2016. Zearalenone as an endocrine disruptor in humans. Environ. Toxicol. Pharmacol. 48, 141–149.
Lephart, E.D., 2015. Modulation of aromatase by phytoestrogens. Enzym. Res. 2015, 594656.
Lo, E.K.K., Wang, X.W., Lee, P.K., Wong, H.C., Lee, J.C.Y., Gomez-Gallego, C., Zhao, D.Y., El-Nezami, H., Li, J., 2023. Mechanistic insights into zearalenone-accelerated colorectal cancer in mice using integrative multi-omics approaches. Comput. Struct. Biotechnol. J. 21, 1785–1796.
Lo, J., Di Nardo, G., Griswold, J., Egbuta, C., Jiang, W.H., Gilardi, G., Ghosh, D., 2013. Structural basis for the functional roles of critical residues in human cytochrome P450 aromatase. Biochemistry 52, 5821–5829.
Louisse, J., Dorne, J., Dellafiora, L., 2022. Investigating the interaction between organic anion transporter 1 and ochratoxin A: an in silico structural study to depict early molecular events of substrate recruitment and the impact of single point mutations. Toxicol. Lett. 355, 19–30.
Ludwig, M, Beck, A, Wickert, L., Bolkenius, U., Tittel, B., Hinkel, K., Bidlingmaier, F. 1998. Female Pseudohermaphroditism Associated with a Novel Homozygous G-to-A (V370-to-M) Substitution in the P-450 Aromatase Gene. 11, 657–664.
Malir, F., Pickova, D., Toman, J., Grosse, Y., Ostry, V., 2023. Hazard characterisation for significant mycotoxins in food. Mycotoxin Res. 39, 81–93.
Martin, G.D.A., Narvaez, J., Bulmer, R., Durrant, M.C., 2016. Biotransformation and molecular docking studies of aromatase inhibitors. Steroids 113, 95–102.
Massart, F., Meucci, V., Saggese, G., Soldani, G., 2008. High growth rate of girls with precocious puberty exposed to estrogenic mycotoxins. J. Pediatr. 152, 690–695.
Massart, F., Saggese, G., 2010. Oestrogenic mycotoxin exposures and precocious pubertal development. Int. J. Androl. 33, 369–376.
Murthy, J.N., Nagaraju, M., Sastry, G.M., Rao, A.R., Sastry, G.N., 2005. Active site acidic residues and structural analysis of modelled human aromatase: A potential drug target for breast cancer. J. Comput. - Aided Mol. Des. 19, 857–870.
Panneerselvam, S., Yesudhas, D., Durai, P., Anwar, M.A., Gosu, V., Choi, S., 2015. A combined molecular docking/dynamics approach to probe the binding mode of cancer drugs with cytochrome P450 3A4. Molecules 20, 14915–14935.
Pedroni, L., Louisse, J., Dorne, J., Dall'Asta, C., Dellafiora, L., 2023a. A computational study on the biotransformation of alkenylbenzenes by a selection of CYPs: Reflections on their possible bioactivation. Toxicology 488, 153471.
Pedroni, L., Louisse, J., Punt, A., Dorne, J., Dall'Asta, C., Dellafiora, L., 2023b. A computational inter-species study on safrole phase i metabolism-dependent bioactivation: a mechanistic insight into the study of possible differences among species. Toxins 15, 94.
Pettersen, E.F., Goddard, T.D., Huang, C.C., Couch, G.S., Greenblatt, D.M., Meng, E.C., Ferrin, T.E., 2004. UCSF chimera - a visualization system for exploratory research and analysis. J. Comput. Chem. 25, 1605–1612.
Pfleger, F., Schwake-Anduschus, C., 2023. Relevance of Zearalenone and its modified forms in bakery products. Mycotoxin Res. 39, 153–163.
Rai, A., Das, M., Tripathi, A., 2020. Occurrence and toxicity of a fusarium mycotoxin, zearalenone. Crit. Rev. Food Sci. Nutr. 60, 2710–2729.
Rivera-Nunez, Z., Barrett, E.S., Szamreta, E.A., Shapses, S.A., Qin, B., Lin, Y., Zarbl, H., Buckley, B., Bandera, E.V., 2019. Urinary mycoestrogens and age and height at menarche in New Jersey girls. Environ. Health 18, 24.
Rizner, T.L., Romano, A., 2023. Targeting the formation of estrogens for treatment of hormone dependent diseases-current status. Front. Pharmacol. 14, 1155558.
Rong, X., Jiang, Y., Li, F., Sun-Waterhouse, D., Zhao, S.C., Guan, X.D., Li, D.P., 2022. Close association between the synergistic toxicity of zearalenone-deoxynivalenol combination and microRNA221-mediated PTEN/PI3K/AKT signaling in HepG2 cells. Toxicology 468, 153104.
Russell, J.F., Wong, J.C., Grumbach, M.M., 2014. Chapter 3J - aromatase deficiency and aromatase excess. In: New, M.I., Lekarev, O., Parsa, A., Yuen, T.T., O'Malley, B.W., Hammer, G.D. (Eds.), Genetic Steroid Disorders. Academic Press, San Diego, pp. 165–190.
Silva, A.S., Brites, C., Pouca, A.V., Barbosa, J., Freitas, A., 2019. UHPLC-ToF-MS method for determination of multi-mycotoxins in maize: Development and validation. Curr. Res. Food Sci. 1, 1–7.
Simpson, E.R., 2000. Genetic mutations resulting in loss of aromatase activity in humans and mice. J. Soc. Gynecol. Investig. 7, S18–S21.
Wang, Y., Liu, T.J., Xie, J.H., Cheng, M.J., Sun, L.R., Zhang, S., Xin, J.Y., Zhang, N., 2022. A review on application of molecular simulation technology in food molecules interaction. Curr. Res. Food Sci. 5, 1873–1881.
Wang, Y.F., Wong, T.Y., Chan, F.L., Chen, S., Leung, L.K., 2014. Assessing the effect of food mycotoxins on aromatase by using a cell-based system. Toxicol. Vitr. 28, 640–646.
Zhang, L., Silva, D.A., Yan, Y.J., Huang, X.H., 2012. Force field development for cofactors in the photosystem II. J. Comput. Chem. 33, 1969–1980.
Zhao, L., Zhang, M.X., Pan, F., Li, J.Y., Dou, R., Wang, X.Y., Wang, Y.Y., He, Y.M., Wang, S.X., Cai, S.B., 2021. In silico analysis of novel dipeptidyl peptidase-IV inhibitory peptides released from Macadamia integrifolia antimicrobial protein 2 (MiAMP2) and the possible pathways involved in diabetes protection. Curr. Res. Food Sci. 4, 603–611.
Zoete, V., Cuendet, M.A., Grosdidier, A., Michielin, O., 2011. SwissParam: a fast force field generation tool for small organic molecules. J. Comput. Chem. 32, 2359–2368.